



Towards Implantable Bio-Supercapacitors: Pseudocapacitance of Ruthenium Oxide Nanoparticles and Nanosheets in Acids, Buffered Solutions, and Bioelectrolytes

Sho Makino,^a Takayuki Ban,^a and Wataru Sugimoto^{a,b,*,z}

^aMaterials and Chemical Engineering, Faculty of Textile Science and Technology, Shinshu University, Ueda, Nagano 386-8567, Japan

^bCenter for Energy and Environmental Science, Interdisciplinary Cluster for Cutting Edge Research, Shinshu University, Ueda, Nagano 386-8567, Japan

Metal oxides, in particular ruthenium-based oxides, are promising electrode materials for aqueous pseudocapacitors. Strong acids or bases are favored over neutral electrolytes owing to the higher capacitance. Here we explore the pseudocapacitive behavior of ruthenium oxide nanoparticles and nanosheets in near neutral pH as an environmentally benign electrolyte. The pseudocapacitive charge storage in poorly-crystalline hydrous RuO₂ nanoparticles, and highly-crystalline RuO₂ nanosheets were investigated in acetic acid-lithium acetate (AcOH-AcOLi) buffered solutions. It is shown that capacitance values as high as 1,038 F g⁻¹ can be achieved in AcOH-AcOLi buffered solutions with RuO₂ nanosheets, which is 44% higher than the benchmark RuO₂ · nH₂O in H₂SO₄ electrolyte (720 F g⁻¹). Furthermore, comparable performance was obtained in phosphate buffered saline and fetal bovine serum. The mechanism of the pseudocapacitive properties is discussed based on the difference in the surface redox behavior of different RuO₂ nanomaterials in acid, neutral, buffered solutions, and in weak acid.

© The Author(s) 2015. Published by ECS. This is an open access article distributed under the terms of the Creative Commons Attribution 4.0 License (CC BY, <http://creativecommons.org/licenses/by/4.0/>), which permits unrestricted reuse of the work in any medium, provided the original work is properly cited. [DOI: 10.1149/2.0021505jes] All rights reserved.

Manuscript submitted December 2, 2014; revised manuscript received December 26, 2014. Published January 9, 2015. *This paper is part of the JES Focus Issue on Electrochemical Capacitors: Fundamentals to Applications.*

Electrochemical capacitors (also known as supercapacitors) are energy harvesting devices capable of charge and discharging within a few seconds, and cycle life in the order of thousands of cycles. Some metal-oxides are known to provide high capacitance in aqueous electrolytes, owing to the combination of the non-faradaic electrical double layer charging and the faradaic surface or near surface confined redox capacitance (pseudocapacitance).¹ Pseudocapacitance is a phenomenon generally observed in aqueous electrolytes.² Acidic or basic electrolytes such as H₂SO₄ and KOH are favorable in terms of power density owing to the high conductivity. RuO₂ is one of the rare oxides that is stable in both acidic and basic conditions. Hydrous RuO₂ nanoparticles (RuO₂ · nH₂O; where *n* is typically 0.5) offers capacitance of ~700 F g⁻¹ in H₂SO₄ electrolyte and can be cycled for thousands of cycles with practically no decay, thus is often used for performance benchmarking of new electrode materials. Although studies on the asymmetric systems and applicability of non-aqueous electrolytes to oxide electrodes in order to widen the operating voltage window have recently been initiated, non-aqueous electrolytes have yet to surpass aqueous electrolytes in terms of specific capacitance.³⁻⁸

Electrolytes near neutral pH are selected for materials that are not as corrosion-resistant in acids and base, for example manganese oxide.⁹⁻¹² Neutral electrolytes are more environmentally benign and its low corrosiveness allows a wider range in choice for periphery material, such as current collectors and packaging.¹³ Despite the RuO₂-based material being the model pseudocapacitive material, studies on the electrochemical capacitor behavior in neutral electrolytes are scarce compared to the more popular acidic or basic electrolytes. One of the reasons is that the capacitance of RuO₂ in neutral electrolytes is generally 1/2 of that in sulfuric acid or potassium hydroxide.¹⁴⁻¹⁷ Nonetheless, the use of neutral pH electrolytes has advantages when used for asymmetric (hybrid) supercapacitors, which are devices that utilize different materials (e.g. metal oxides, carbon, etc) for the positive and negative electrodes.¹² In such a case, the operating voltage window can be extended beyond the thermodynamic 1.2 V limit if the kinetics of gas evolution is extremely slow. Up to now, alkali metal sulfates, nitrates, and chlorides have been used as neutral electrolytes.

We have also used Li₂SO₄ as the electrolyte for our hybrid supercapacitors based on protected Li anode technology.¹⁸⁻²⁰ This hybrid supercapacitor utilizes a Li ion conducting glass ceramic membrane, which is stable within a limited pH range. We recently communicated that unprecedented capacitance values exceeding that of H₂SO₄ can be achieved by using an acetic acid-lithium acetate (AcOH-AcOLi) buffered solution with near neutral pH,²⁰ suggesting the possibility of other new electrolytes.

In this study, emphasis was placed on elucidating the origin and mechanism of the pseudocapacitance of ruthenium based oxides in buffered solutions. Three different nanostructured RuO₂ materials were studied; namely poorly crystalline hydrous RuO₂ nanoparticles, well-crystalline anhydrous RuO₂ nanoparticles, and crystalline RuO₂ nanosheets. The capacitive behavior of these materials were studied in H₂SO₄ as the acidic electrolyte, or Li₂SO₄ or AcOLi as neutral electrolyte. Various AcOH-AcOLi buffer solutions with different ionic strength (constant pH) were used, and the ratio of weak acid/conjugated base ratio was also varied. In addition, the role of weak acid was investigated by adding a small amount of AcOH to a supporting electrolyte (Li₂SO₄). Furthermore, phosphate buffered saline and fetal bovine serum were studied as bioelectrolytes for application toward implantable bio-supercapacitors.

Experimental

Ultrapure water (Milli-Q, >18 MΩ cm) was used for all synthesis and characterization. RuO₂ · nH₂O was prepared by a modified sol-gel process following literature.^{21,22} In a typical synthesis, a 0.3 M NaOH solution was slowly added to a 0.1 M aqueous RuCl₃ solution while maintaining a constant pH value of 7. The precipitate was collected and washed thoroughly to remove by-products. The product was suspended in H₂O and aged for 72 h at 40°C. The powder samples were collected and heat treated in air at 150°C for 17 h to obtain RuO₂ · nH₂O (*n* = 0.5). Anhydrous RuO₂ was prepared by calcination of RuO₂ · xH₂O (Johnson Matthey) at 450°C for 2 h.

Ruthenium oxide nanosheets (RuO₂ns) were synthesized following a previously reported method.²³ Briefly, α-NaFeO₂ type NaRuO₂ was synthesized by solid state reaction of Na₂CO₃, Ru and RuO₂ (2: 1: 3 molar ratio) at 900°C for 12 h under Ar atmosphere. Oxidative

*Electrochemical Society Active Member.

^zE-mail: wsugi@shinshu-u.ac.jp

Table I. List of buffered solutions used.

Electrolyte	Mixing volume ratio	pH	Conductivity/ S m ⁻¹
0.5 M AcOH - AcOLi	12.5 : 87.5	5.4	2.15
2.0 M AcOH - AcOLi	12.5 : 87.5	5.4	3.35
2.0 M AcOH - AcOLi	58.5 : 41.5	4.4	3.04
2.0 M AcOH - AcOLi	95.0 : 5.0	3.3	0.586
5.0 M AcOH - AcOLi	12.5 : 87.5	5.4	3.76
0.1 M AcOH + 1.0 M Li ₂ SO ₄	5.0 : 95.0	4.2	6.87
Phosphate buffered saline	–	7.3	–
Fetal bovine serum	–	7.4	–

de-intercalation of Na⁺ with aqueous Na₂S₂O₈ and subsequent proton exchange in 1 M HCl leads to the layered H_{0.2}RuO₂ · 0.5H₂O. The layered ruthenic acid was added to a tetrabutylammonium hydroxide (TBAOH) aqueous solution with the molar ratio of TBA ions to the exchangeable protons in H_{0.2}RuO₂ · 0.5H₂O adjusted to TBA⁺/H⁺ = 5. The dispersion was vigorously shaken for 10 days to exfoliate the layered ruthenate into elementary RuO₂ nanosheets. The resultant suspension was centrifuged at 2,000 rpm for 30 min to remove trace amounts of impurity Ru metal and non-exfoliated material.

Electrochemical measurements were carried out using a beaker-type electrochemical cell composed of a Pt mesh counter electrode and a Ag/AgCl/KCl (sat.) reference electrode connected with a salt bridge. A Luggin capillary faced the working electrode at a distance of 2 mm. Electrode potentials will be referred to the reversible hydrogen electrode (RHE) potential scale. The working electrodes for RuO₂ · nH₂O and anhydrous RuO₂ was prepared by coating the active material on a glassy carbon surface (~200 μg cm⁻²). A thin layer of Nafion ionomer was cast on the electrode as a proton conductive binder. Re-stacked RuO₂ nanosheet electrodes were prepared by dropping a colloidal suspension onto a mirror-polished glassy carbon rod (~20 μg cm⁻²). The capacitance was calculated by averaging the anodic and cathodic charge. Cyclic voltammetry was conducted in H₂SO₄, Li₂SO₄, AcOLi, and AcOH-AcOLi at 60°C unless otherwise noted with the scan rate 2, 5, 20, 50, 200, 500 mV s⁻¹. Phosphate

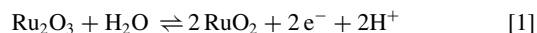
buffered saline and fetal bovine serum (Biowest, France) was used as-received. The electrolytes used in this study are summarized in Table I.

Results and Discussion

Impact of electrolyte on the pseudocapacitive properties of RuO₂ · nH₂O.— Cyclic voltammograms of RuO₂ · nH₂O nanoparticles in 0.5 M H₂SO₄, 1.0 M Li₂SO₄, 2.0 M AcOLi, and 2.0 M AcOH-AcOLi are shown in Fig. 1A. The voltammograms in 0.5 M H₂SO₄ are typical of sol-gel derived RuO₂ · nH₂O nanoparticles with a maximum capacitance of 720 F g⁻¹ at 2 mV s⁻¹, decreasing by 18% to 589 F g⁻¹ at 500 mV s⁻¹. A broad redox peak at E_{1/2} = 0.60 V vs RHE can be clearly distinguished.

The cyclic voltammograms in 1.0 M Li₂SO₄ are characterized by a rectangular background current (shown as shaded region in the figure), and a slow irreversible redox process above 0.8 V and below 0.6 V vs RHE on the anodic and cathode scans, respectively. The rectangular background current is superimposed for the other electrolytes assuming that the C_{dl} is the same regardless of electrolyte. Here we are disregarding the size of the (solvated) ions for sake of simplicity. The specific capacitance due to electrical double layer charging (C_{dl}) in 1.0 M Li₂SO₄ is estimated as ~200 F g⁻¹ from the scan rate independent region. This capacitance translates to an estimated surface area of 1,000 m² g⁻¹ or 1.0 nm particle size, taking the value of 20 μF cm⁻² as a probe value for area specific capacitance. This particle size is in good agreement with the local structure derived by EXFAS²⁴ and SAXS.²⁵

The pseudocapacitance due to surface redox processes (C_{redox}) is calculated by subtracting C_{dl} from the overall capacitance C at the respective scan rates and is shown in Fig. 1B. The slow irreversible redox process above 0.8 V and below 0.6 V can be interpreted as the dissociative adsorption of water according to reaction 1.^{15,16}



The behavior in 2.0 M AcOLi is similar to Li₂SO₄ in many aspects. The C_{dl} values in AcOLi and Li₂SO₄ are both ~200 F g⁻¹. The redox peaks due to reaction 1 is observed at E_{1/2} = 0.70 V, which is close

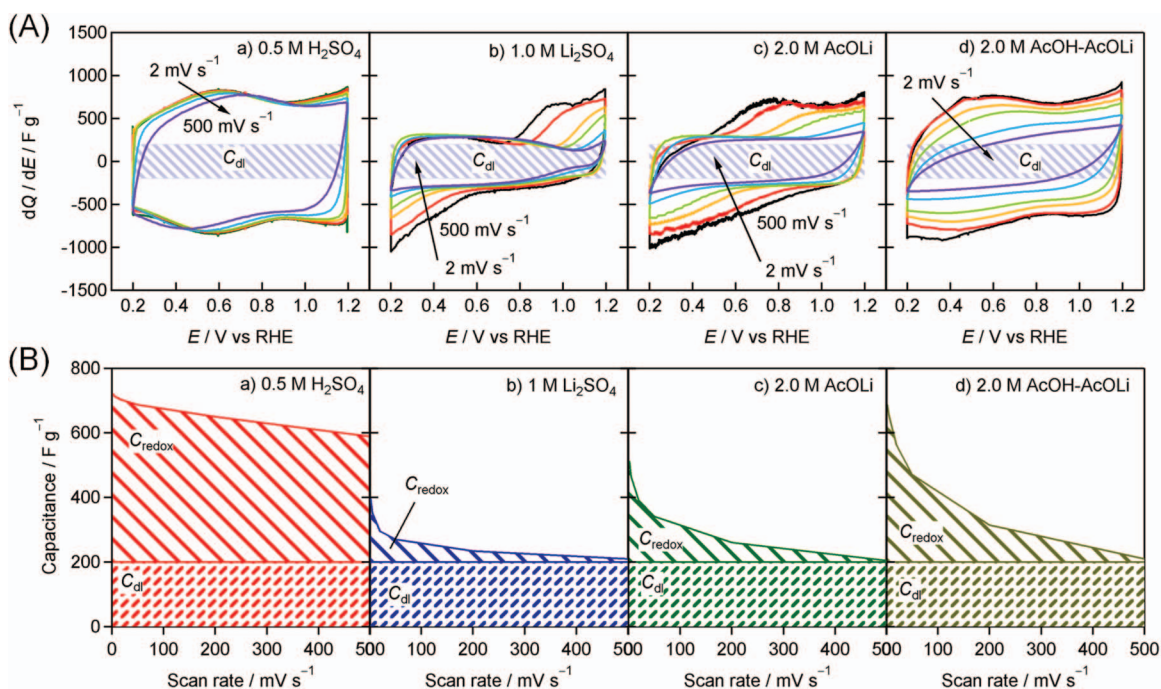


Figure 1. (A) Cyclic voltammograms of RuO₂ · nH₂O in a) 0.5 M H₂SO₄, b) 1.0 M Li₂SO₄, c) 2.0 M AcOLi, and d) 2.0 M AcOH-AcOLi at 60°C with $\nu = 2, 5, 20, 50, 200, \text{ and } 500 \text{ mV s}^{-1}$. (B) The overall capacitance deconvoluted into the electrical double layer capacitance ($C_{dl} = 200 \text{ F g}^{-1}$) and redox capacitance (C_{redox}).

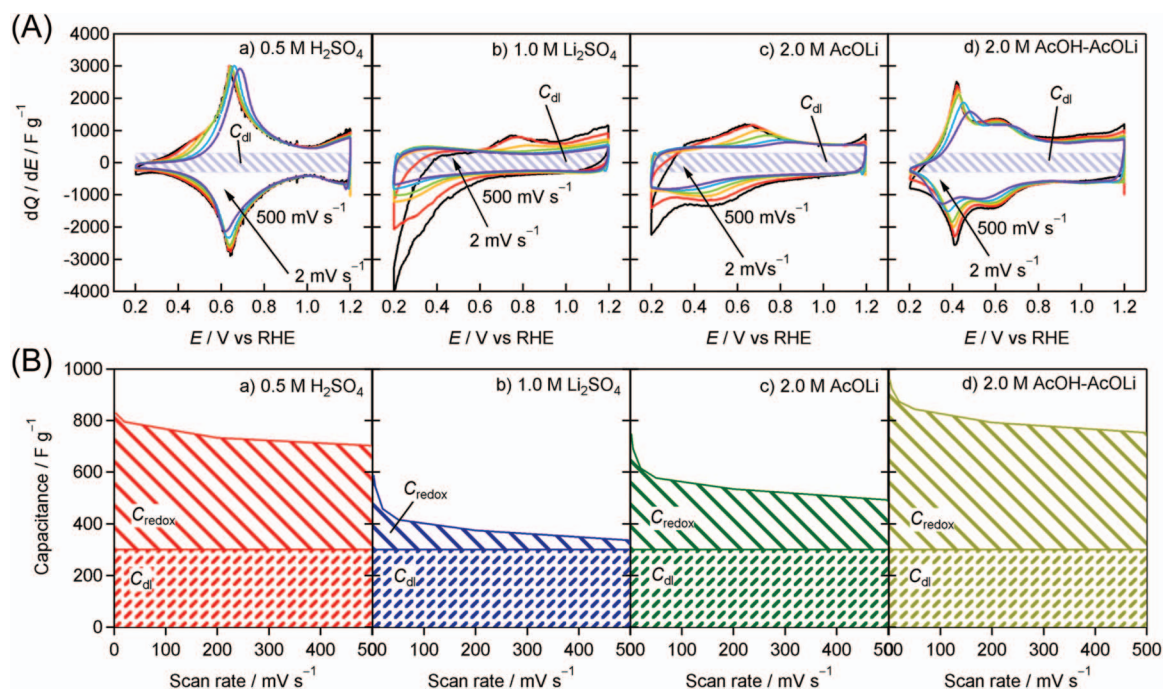


Figure 2. (A) Cyclic voltammograms of RuO₂ nanosheets in a) 0.5 M H₂SO₄, b) 1.0 M Li₂SO₄, c) 2.0 M AcOLi, and d) 2.0 M AcOH-AcOLi at 60°C with $\nu = 2, 5, 20, 50, 200,$ and 500 mV s^{-1} . (B) The overall capacitance deconvoluted into the electrical double layer capacitance ($C_{dl} = 300 \text{ F g}^{-1}$) and redox capacitance (C_{redox}).

to the Ru⁴⁺/Ru³⁺ potential according to the Pourbaix diagram²⁶ for this reaction. An obvious difference is the charge related to reaction 1; The charge is higher in 2.0 M AcOLi. This difference may be due to specific adsorption of SO₄²⁻ on the oxide surface, hindering the adsorption of water, and thus delaying reaction 1.

The behavior in 2.0 M AcOH-AcOLi seems to be a combination of the behavior in H₂SO₄ and AcOLi depending on the scan rate. At slow scan rates the voltammograms are similar to that in H₂SO₄ and a capacitance of 687 F g⁻¹ at 2 mV s⁻¹ is obtained. On the other hand, only electrical double layer charging occurs at fast scan rates in AcOLi, reducing the capacitance to 210 F g⁻¹ at 500 mV s⁻¹. This phenomenon (lack of pseudocapacitance at high scan rates) is due to the low proton concentration in 2.0 M AcOH-AcOLi. Surface redox process related with hydrated protons will become diffusion limited at high scan rates. If we take the C_{dl} values of ~200 F g⁻¹ from AcOLi, C_{redox} in 2.0 M AcOH-AcOLi becomes extremely large (487 F g⁻¹ or 64.8 kC mol⁻¹). Dividing 64.8 kC mol⁻¹ by the Faraday constant 96.5 kC mol⁻¹ gives a 0.6 electron reaction for C_{redox} . Since not all of the Ru ions will be in the outer shell of the nanoparticle, this value seems to be a reasonable value for pseudocapacitance.

Using the C_{dl} values obtained in neutral electrolytes, we can calculate the C_{redox} in 0.5 M H₂SO₄ as 400–500 F g⁻¹. The $E_{1/2} = 0.60 \text{ V}$ vs RHE in H₂SO₄ is also attributed to reaction 1.¹⁶ Note that if we take differential capacitance that is mostly scan-rate independent in H₂SO₄ as the C_{dl} (which is often practiced in literature (see for example ref [27,28])), C_{dl} can be estimated as 500 F g⁻¹. The probe value of 80 μF cm⁻² is often used as a measure of the specific capacitance in H₂SO₄, which originates from the above mentioned treatment. The results and discussion shown here using various electrolytes suggests that this probe value contains both C_{dl} and C_{redox} charge.

The pseudocapacitive behavior of anhydrous RuO₂ nanoparticles in 0.5 M H₂SO₄, 1.0 M Li₂SO₄, 2.0 M AcOLi, and 2.0 M AcOH-AcOLi are qualitatively similar to RuO₂ · nH₂O (Fig. S1). The change in molarity of AcOH-AcOLi between 0.5 and 5.0 M does not affect the voltammograms significantly (Fig. S2). At the lowest concentration of 0.5 M, a peak at $E_{1/2} = 0.41 \text{ V}$ evolves at slow scan rate, which is attributable to the adsorption of AcOH (discussed in detail later).

Pseudocapacitive properties of RuO₂ nanosheets in various electrolytes.— Cyclic voltammograms of RuO₂ nanosheets in 0.5 M H₂SO₄, 1.0 M Li₂SO₄, 2.0 M AcOLi, and 2.0 M AcOH-AcOLi are shown in Fig. 2A. The voltammograms in 0.5 M H₂SO₄ are quite different from sol-gel derived RuO₂ · nH₂O nanoparticles in that there is a distinctive large redox pair at $E_{1/2} = 0.64 \text{ V}$ vs. RHE. The capacitance at 2 mV s⁻¹ is 831 F g⁻¹ and decreases by 15% to 703 F g⁻¹ at 500 mV s⁻¹. Following the case for RuO₂ · nH₂O nanoparticles, the C_{dl} value can be deduced from the constant dQ/dE background current taken in Li₂SO₄, which is $C_{dl} \sim 300 \text{ F g}^{-1}$. The deconvoluted C_{dl} and C_{redox} contribution at the respective scan rates are given in Fig. 2B. Using the C_{dl} value and 20 μF cm⁻², the electrochemically accessible surface area is estimated as 1,500 m² g⁻¹. This is much higher than the theoretical surface area of ~400 m² g⁻¹ for a RuO₂ nanosheet crystallite with thickness of 0.7 nm. The estimated $C_{dl} \sim 300 \text{ F g}^{-1}$ most likely includes pseudocapacitance from fast surface redox processes. C_{redox} due to reaction 1 is observed also for RuO₂ nanosheets in Li₂SO₄ and AcOLi, although the contribution is much smaller than for RuO₂ · nH₂O nanoparticles. The cathodic current below 0.6 V and corresponding oxidation current at $E = 0.75 \text{ V}$ in Li₂SO₄ and AcOLi (Fig. 2A(b) and (c)) may be due to hydrogen adsorption.²⁸ The behavior of RuO₂ nanosheets in 2.0 M AcOH-AcOLi is characterized by two pairs of redox peaks at $E_{1/2} = 0.41$ and 0.60 V vs RHE. The former pair is more scan rate dependent than the latter. The overall capacitance is 958 F g⁻¹ at 2 mV s⁻¹ and 752 F g⁻¹ at 500 mV s⁻¹. The C_{redox} in H₂SO₄ and AcOH-AcOLi represents 50 to 70% of the overall capacitance.

The distinctive redox peaks observed for RuO₂ nanosheets changes drastically when the ionic strength of the AcOH-AcOLi buffer solution is changed while keeping a constant pH (Fig. S3).²⁰ The redox pair at $E_{1/2} = 0.41 \text{ V}$ is strongly dependent on the ionic strength, broadening and decreasing in charge with decreasing AcOH-AcOLi concentration. The $E_{1/2} = 0.60 \text{ V}$ peak is less dependent on the AcOH-AcOLi concentration. These observations can be attributed to decreasing concentration of the active species. It is noted that at the highest concentration of 5.0 M AcOH-AcOLi, a remarkable capacitance of 1,038 F g⁻¹ is obtained.²⁰

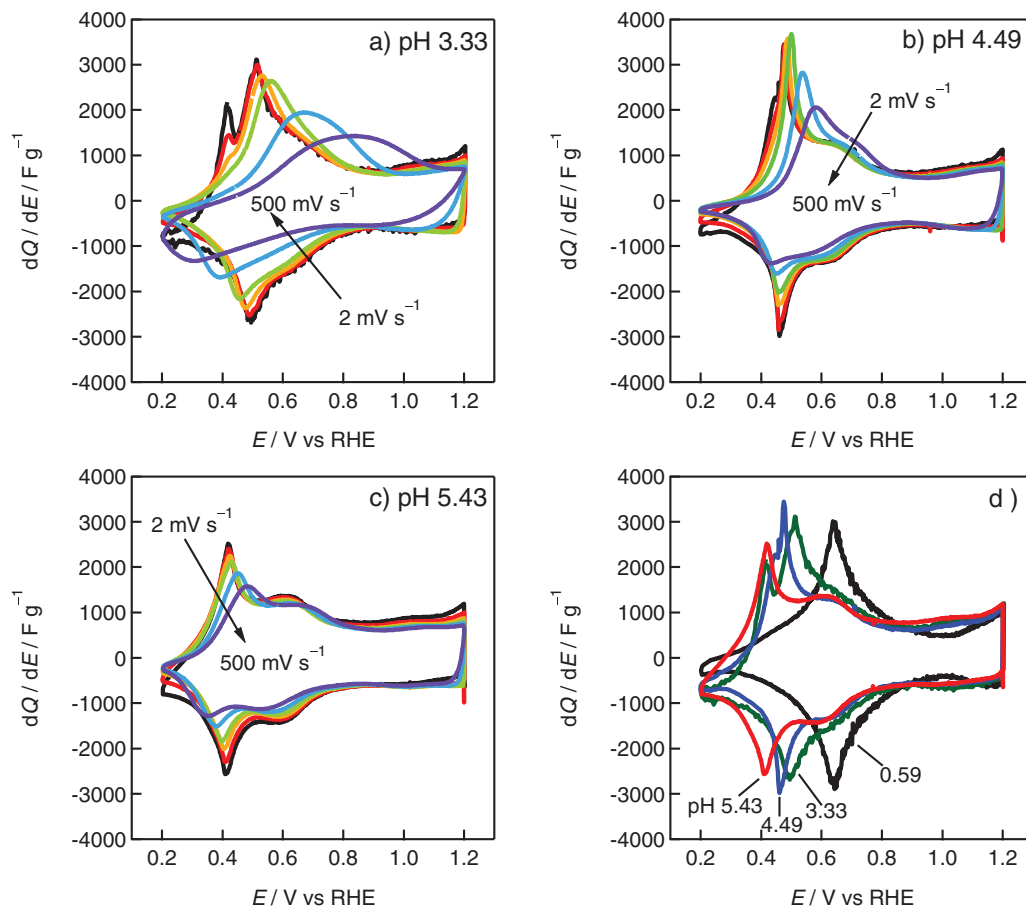


Figure 3. Cyclic voltammograms of RuO₂ nanosheets at 2, 5, 20, 50, 200, 500 mV s⁻¹ in 2.0 M AcOH-AcOLi at pH of a) 3.33, b) 4.49, and c) 5.43. d) Cyclic voltammograms of RuO₂ nanosheet at 2 mV s⁻¹ in 2.0 M AcOH-AcOLi with various pH and 0.5 M H₂SO₄.

In order to gain further insight into the origin of the redox peaks, the pH of the buffer solution was controlled by changing the salt/supporting electrolyte volumetric ratio. As shown in Fig. 3, as the pH is lowered, the cyclic voltammograms become strongly scan rate dependent, which is due to the decrease in the conductivity of the buffer solutions. Figure 3d compares the voltammograms at 2 mV s⁻¹. The $E_{1/2} = 0.60$ V vs RHE peak is independent of pH (note that in H₂SO₄, the $E_{1/2} = 0.41$ and 0.60 V vs RHE peaks overlap). The $E_{1/2} = 0.60$ V vs RHE peak is attributed to reaction 1, similar to the case for RuO₂ · nH₂O nanoparticles. The $E_{1/2} = 0.41$ V vs RHE (at pH = 5.43) shifts to positive potentials as the pH is decreased. This peak shows a linear relation with pH (Fig. 4), suggesting that it is related to adsorption of protons or hydrated protons. Analysis of the slope shows that this is a 1.5 electron reaction, or 3 electrons per 2 reaction sites. This irregular behavior is consistent with previous studies on hydrous metal oxide films of Ir and Ru.²⁹⁻³¹

Figure 5 shows comparative data of the change in pH for RuO₂ · nH₂O nanoparticles. The cyclic voltammograms for H₂SO₄ and 2.0 M AcOH-AcOLi (pH = 5.36) completely overlap, suggesting an analogous charge storage mechanism. On the other hand, the electrochemical behavior in 2.0 M AcOH-AcOLi with pH = 4.44 and 3.42 are quite different. For pH = 3.42, the electrical double layer capacitance is completely lost. We attribute this peculiarity to adsorption of molecular AcOH (not AcO⁻) on the surface of RuO₂, blocking the electrical double layer formation. As the pH is lowered, the relative content of AcOH increases (Table I). In the case of 2.0 M AcOH-AcOLi (pH = 5.36), the adsorption of AcOH is not evident since the concentration of AcOH is much smaller than at pH = 4.44 and 3.42. A similar phenomena was observed for adsorption of CH₃OH in H₂SO₄, where CH₃OH is adsorbed on RuO₂ · nH₂O nanoparticles.²³

The reason for the absence of AcOH adsorption on RuO₂ nanosheets cannot be identified at this point, but it should be noted that CH₃OH also does not adsorb on RuO₂ nanosheets.²³

A weak acid in a supporting electrolyte.— Figure 6 shows cyclic voltammograms when a small amount of AcOH was added to Li₂SO₄ (0.1 M AcOH + 1.0 M Li₂SO₄, pH = 4.16). At slow scan rates

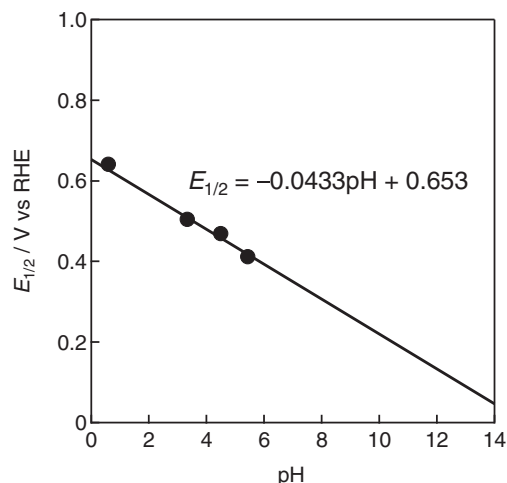


Figure 4. Plots of $E_{1/2}$ of redox peaks for RuO₂ nanosheets in 2.0 M AcOH-AcOLi and 0.5 M H₂SO₄ as a function of the pH.

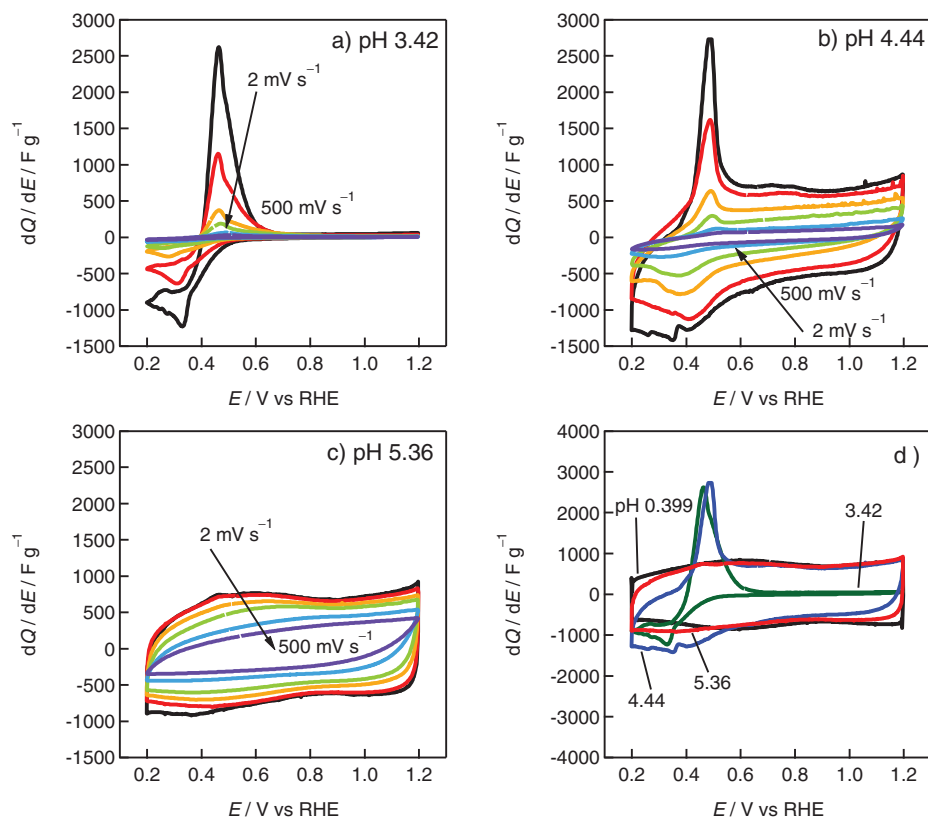


Figure 5. Cyclic voltammograms of $\text{RuO}_2 \cdot n\text{H}_2\text{O}$ at 2, 5, 20, 50, 200, 500 mV s^{-1} in 2.0 M AcOH-AcOLi at pH of a) 3.42, b) 4.44, and c) 5.36. d) Cyclic voltammograms of RuO_2 nanosheets at 2 mV s^{-1} in 2.0 M AcOH-AcOLi with various pH and 0.5 M H_2SO_4 .

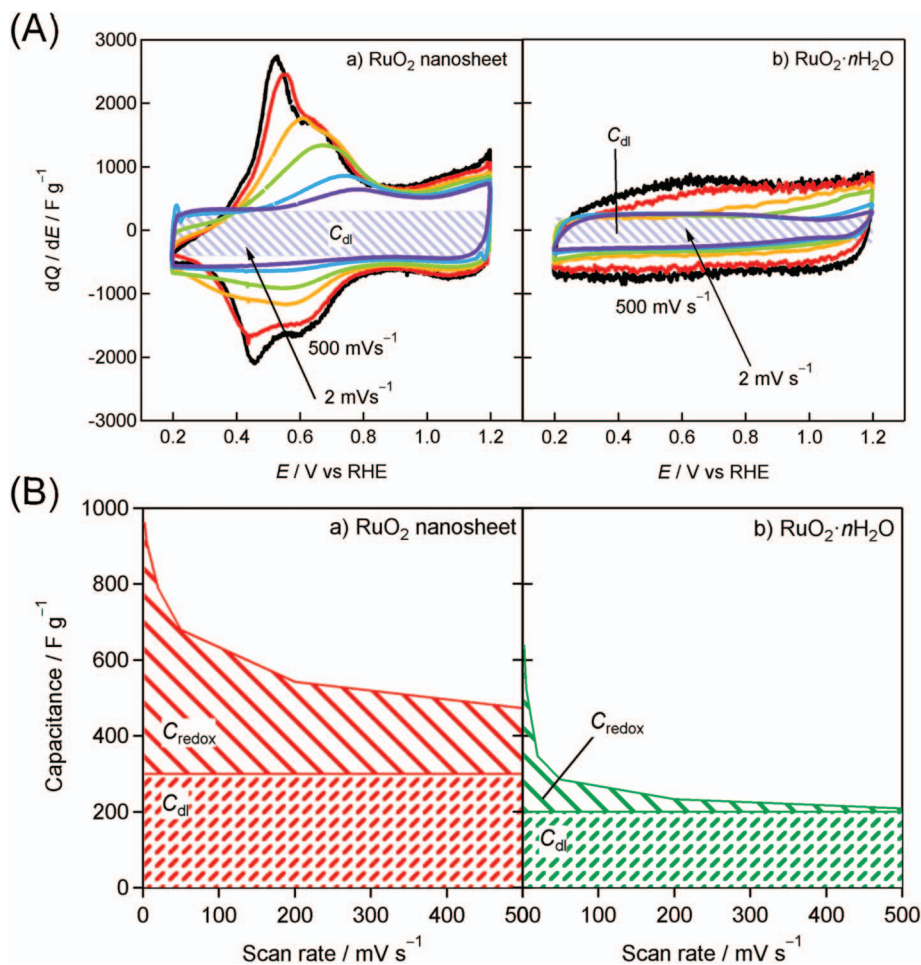


Figure 6. (A) Cyclic voltammograms and (B) deconvoluted of specific capacitance for a) RuO_2 nanosheets and b) $\text{RuO}_2 \cdot n\text{H}_2\text{O}$ in 0.1 M AcOH-1.0 M Li_2SO_4 (pH 4.16).

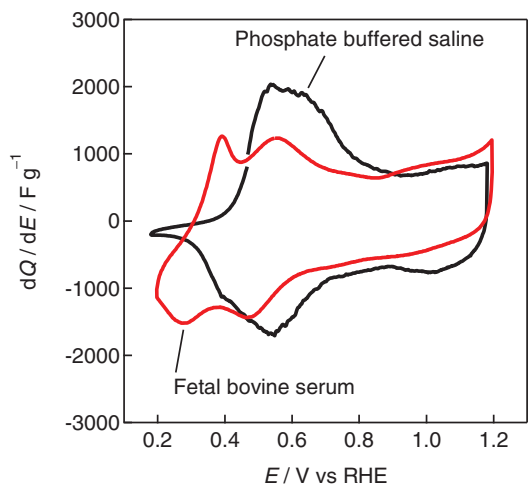


Figure 7. Cyclic voltammograms of RuO₂ nanosheets at 2 mV s⁻¹ in phosphate buffered saline and fetal bovine serum at 25°C.

the cyclic voltammograms for RuO₂ · nH₂O nanoparticles and RuO₂ nanosheets both resemble the behavior in AcOH-AcOLi buffered solutions. The capacitance at 2 mV s⁻¹ is 639 and 962 F g⁻¹ for RuO₂ · nH₂O nanoparticles and RuO₂ nanosheets, respectively. On the other hand, at fast scan rate, the voltammograms are similar to those in Li₂SO₄, since the concentration of AcOH is very small. This clearly shows that protons contribute to the pseudocapacitive behavior of RuO₂-based nanostructures. Thus, an electrolyte composed of a weak acid and a supporting electrolyte can also be used as an electrolyte for pseudocapacitors. Buffered solutions have the advantage of pH control, ionic strength, and biocompatibility, compared to a weak acid in supporting electrolyte. However, the finding that such a simple mixture can be used as an electrolyte for pseudocapacitors paves the way to a massive combination of new electrolytes to explore.

Bio-supercapacitor based on phosphate buffered saline and fetal bovine serum.— Besides the benefit of control in pH and ionic strength, buffered solutions have the advantage of biocompatibility, as many buffers exist in nature (sea water, blood, internal cell fluids, cells and tissues). Here we demonstrate the use of phosphate buffered saline and fetal bovine serum as bioelectrolytes for supercapacitors applicable to safe and bio-compatible implantable power sources. Figure 7 shows the cyclic voltammograms of RuO₂ nanosheets in phosphate buffered saline and fetal bovine serum at 25°C. The redox behavior and capacitance are similar to the AcOH-AcOLi system. The specific capacitance at 2 mV s⁻¹ in phosphate buffered saline was 837 F g⁻¹, and 772 F g⁻¹ in fetal bovine serum. These values are at least twice as large as those of MWCNTs/PANI composite in physiological electrolyte and human serum.³² The results potentially show that the combination of pseudocapacitive oxide electrodes and bioelectrolytes can afford exceptionally high energy density.

Conclusions

The electrochemical charge storage in buffered solutions using poorly-crystalline hydrous RuO₂ nanoparticles and well-crystalline RuO₂ nanosheets as electrode materials was studied. Capacitance comparable to or higher than H₂SO₄ were obtained in acetic acid-lithium acetate (AcOH-AcOLi) buffered solutions, depending on the ionic strength and pH. At constant pH, AcOH-AcOLi with higher ionic strength (molarity) lead to higher capacitance, owing to the presence of higher concentration of the adsorbant in the electrolyte. When the pH is varied by changing the volume ratio of AcOH-AcOLi, the pseudocapacitive behavior deteriorated with decreasing pH. This phenomenon is discussed based on the decrease in the conductivity of the electrolyte. The highest capacitance of 1,038 F g⁻¹ was obtained in a

5 M AcOH-AcOLi (pH = 5.4) with RuO₂ nanosheet electrodes. RuO₂ nanosheets afforded 20 to 50% higher capacitance than RuO₂ · nH₂O in all of the electrolytes studied (H₂SO₄, Li₂SO₄, AcOLi, AcOH-AcOLi, AcOH-Li₂SO₄). The lower capacitance of RuO₂ · nH₂O in AcOH-AcOLi is due to the adsorption of AcOH molecules, which hinders the formation of the electrical double layer. Moreover, outstanding performance was obtained in phosphate buffered saline (837 F g⁻¹) and fetal bovine serum (772 F g⁻¹) with RuO₂ nanosheet electrodes. The results presented here demonstrate the effective use of bioelectrolytes for pseudocapacitors applicable to environmentally benign, safe and bio-compatible implantable power sources.

Acknowledgments

This work was supported in part by the Advanced Low Carbon Technology Research and Development Program (ALCA) of the Japan Science and Technology Agency (JST) and Chubu Electric Power Co., Inc. W.S. wishes to thank Profs. Akira Teramoto and Koji Abe of Shinshu University for fruitful discussion on the bioelectrolytes. This manuscript is dedicated to the memory of Professor Koji Abe, an excellent researcher and a humble and modest colleague, who passed away suddenly on 18 November, 2014, during the course of the preparation of this manuscript.

References

- B. Conway, *Electrochemical supercapacitors: scientific fundamentals and technological applications*, Kluwer Academic/Plenum Publishers, New York, USA, (1999).
- V. Augustyn, P. Simon, and B. Dunn, *Energy Environ. Sci.*, **7**, 1597 (2014).
- V. Augustyn, J. Come, M. a Lowe, J. W. Kim, P.-L. Taberna, S. H. Tolbert, H. D. Abruña, P. Simon, and B. Dunn, *Nat. Mater.*, **12**, 518 (2013).
- M. Egashira, T. Uno, N. Yoshimoto, and M. Morita, *Electrochemistry*, **75**, 595 (2007).
- S. Makino, Y. Takasu, and W. Sugimoto, *Chem. Lett.*, **39**, 544 (2010).
- L. Mayrand-Provencher, S. Lin, D. Lazzarini, and D. Rochefort, *J. Power Sources*, **195**, 5114 (2010).
- D. Rochefort and A.-L. Pont, *Electrochem. Commun.*, **8**, 1539 (2006).
- K.-H. Chang, C.-C. Hu, C.-M. Huang, Y.-L. Liu, and C.-I. Chang, *J. Power Sources*, **196**, 2387 (2011).
- H. Y. Lee and J. B. Goodenough, *J. Solid State Chem.*, **148**, 81 (1999).
- H. Y. Lee, V. Manivannan, and J. B. Goodenough, *Comptes Rendus l'Académie des Sci. - Ser. IIC - Chem.*, **2**, 565 (1999).
- H. Y. Lee and J. B. Goodenough, *J. Solid State Chem.*, **144**, 220 (1999).
- J. W. Long, D. Bélanger, T. Brousse, W. Sugimoto, M. B. Sassin, and O. Crosnier, *MRS Bull.*, **36**, 513 (2011).
- Z. Chang, Y. Yang, M. Li, X. Wang, and Y. Wu, *J. Mater. Chem. A*, **2**, 10739 (2014).
- S. Wen, J. Lee, I. Yeo, J. Park, and S. Mho, *Electrochim. Acta*, **50**, 849 (2004).
- S. Sopčić, Z. Mandić, G. Inzelt, M. K. Roković, and E. Meštrović, *J. Power Sources*, **196**, 4849 (2011).
- S. Sopčić, M. K. Roković, Z. Mandić, A. Róka, and G. Inzelt, *Electrochim. Acta*, **56**, 3543 (2011).
- M. Tomkiewicz, Y. S. Huang, F. H. Pollak, and J. E. Soc, *J. Electrochem. Soc.*, **130**, 1514 (1983).
- W. Shimizu, S. Makino, K. Takahashi, N. Imanishi, and W. Sugimoto, *J. Power Sources*, **241**, 572 (2013).
- S. Makino, Y. Shinohara, T. Ban, W. Shimizu, K. Takahashi, N. Imanishi, and W. Sugimoto, *RSC Adv.*, **2**, 12144 (2012).
- S. Makino, T. Ban, and W. Sugimoto, *Electrochemistry*, **81**, 795 (2013).
- J. P. Zheng and T. R. Jow, *J. Electrochem. Soc.*, **142**, L6 (1995).
- J. P. Zheng, P. J. Cygan, and T. R. Jow, *J. Electrochem. Soc.*, **142**, 2699 (1995).
- K. Fukuda, T. Saida, J. Sato, M. Yonezawa, Y. Takasu, and W. Sugimoto, *Inorg. Chem.*, **49**, 4391 (2010).
- D. A. McKeown, P. L. Hagans, L. P. L. Carette, A. E. Russell, K. E. Swider, and D. R. Rolison, *J. Phys. Chem. B*, **103**, 4825 (1999).
- N. Yoshida, Y. Yamada, S. Nishimura, Y. Oba, M. Ohnuma, and A. Yamada, *J. Phys. Chem. C*, **117**, 12003 (2013).
- M. Pourbaix, *Atlas of Electrochemical Equilibria in Aqueous Solutions*, 2nd ed., National Association of Corrosion Engineers, Houston, Tex, (1974).
- W. Sugimoto, K. Yokoshima, Y. Murakami, and Y. Takasu, *Electrochim. Acta*, **52**, 1742 (2006).
- W. Sugimoto, T. Kizaki, K. Yokoshima, Y. Murakami, and Y. Takasu, *Electrochim. Acta*, **49**, 313 (2004).
- L. D. Burke and O. J. Murphy, *J. Electroanal. Chem. Interfacial Electrochem.*, **109**, 199 (1980).
- L. D. Burke, M. E. Lyons, E. J. M. O'Sullivan, and D. P. Whelan, *J. Electroanal. Chem. Interfacial Electrochem.*, **122**, 403 (1981).
- L. D. Burke and J. F. Healy, *J. Electroanal. Chem. Interfacial Electrochem.*, **124**, 327 (1981).
- M. Ammam and J. Fransaer, *Chem. Commun.*, **48**, 2036 (2012).